Coulomb-driven cluster-glass behavior in Mn-intercalated Ti_{1+y}S_{2}

P. M. Shand, A. L. Meyer, M. Streicher, A. Wilson, T. Rash, M. W. Roth, T. E. Kidd, and L. H. Strauss

Phys. Rev. B **85**, 144432 — Published 27 April 2012

DOI: 10.1103/PhysRevB.85.144432

Coulomb-driven cluster-glass behavior in Mn-intercalated $Ti_{1.1}S_2$

P. M. Shand, A. L. Meyer, M. Streicher, A. Wilson, T. Rash, M. W. Roth, T. E. Kidd
Physics Department, University of Northern Iowa, Cedar Falls, IA 50614-0150

L. H. Strauss
Department of Chemistry and Biochemistry, University of Northern Iowa, Cedar Falls, IA 50614-0423

Receipt Date: 8/3/2011

ABSTRACT

We have investigated the low-temperature spin-glass-like phase in the intercalated transition-metal dichalcogenide $Mn_{0.09}Ti_{1.1}S_2$. A departure from Curie-Weiss behavior in the paramagnetic regime indicated the formation of small ferromagnetically-correlated clusters. The Vogel-Fulcher law provided an excellent description of relaxation times in the vicinity of the transition, showing that the glass-like phase occurs due to interaction between the clusters. Cole-Cole plots for data close to the transition were linear, which is consistent with a simple exponential distribution of cluster sizes. A Monte Carlo simulation of the dichalcogenide system including excess self-intercalated Ti ions gave an exponential cluster-size distribution for a relatively narrow range of concentration values of Mn and Ti ions, values that were consistent with those of the $Mn_{0.09}Ti_{1.1}S_2$ sample. Strong commonality in the relaxation behavior with certain ferroelectric relaxor systems suggests underlying similarity in the microscopic structure of the clusters in both systems, which may be chain-like or quasi-one-dimensional.

PACS Numbers: 75.30.Hx, 75.50.Lk, 76.60.Es, 77.80.-e

I. INTRODUCTION

Intercalated transition-metal dichalcogenides (TMDCs) have been the subject of numerous experimental and theoretical studies over the past several decades.[1-6] These materials exhibit a variety of electronic and magnetic properties resulting from the interplay between the quasi-two-dimensional anisotropic layered structure of the host and the electronic and magnetic characteristics of the intercalated ions. The intercalant ions are incorporated in the van der Waals gaps between the Ch-T-Ch trilayer slabs, which are stacked along the *c* axis. (T signifies transition metal and Ch denotes chalcogen.) The occurrence of a charge density wave state in $TiSe_2$, its suppression by intercalation and the accompanying enhancement of superconductivity is one of the most intriguing aspects of the electronic and magnetic characteristics of the TMDCs.[7-9] Other notable intercalation-dependent characteristics encompass a wide array of magnetic phases including ferromagnetism, antiferromagnetism, and spin-glass or cluster-glass states.[10-15]

The multiplicity of magnetic states arises because of the type of magnetic intercalant ion, the interactions between the intercalant ions, band-structure effects due to the intercalation, and the distribution of the intercalant ions. Intercalation of 3*d* transition-metal ions such as Mn or Fe results in localized moments (especially for Mn). In a host TMDC that is a metal (e.g., TaS_2) or a degenerate semiconductor (e.g., TiS_2), the intercalated moments interact via Ruderman-Kittel-Kasuya-Yosida (RRKY) exchange, which is mediated by electrons in *d* or *p-d* bands at the Fermi level. The 3*d* intercalant atoms donate electrons to the conduction band thereby becoming divalent or trivalent ions and simultaneously increasing the carrier density of the material. The magnetic moments may also interact via superexchange, which likely stabilizes the

antiferromagnetic state in some intercalated TMDCs.[10] At 25 atomic percent and 33 atomic percent concentrations, the intercalant ions can form ordered $2a \times 2a$ and $\sqrt{3}a \times \sqrt{3}a$ superlattices, respectively, where *a* is the in-plane lattice parameter.[1, 2] At other concentrations, the intercalants form short-range ordered structures. In the particular case of TiS_2, the fabrication process results in significant self-intercalation of Ti atoms.[16-18] As an intercalant, Ti tends to form Ti^{3+} or Ti^{4+} ions.[17] These highly charged ions will alter the distribution of the magnetic ions that may also be present as intercalants, which in turn will impact the magnetic characteristics of the system.[6]

In this paper, we present experimental evidence that the spin-glass-like relaxation behavior that we have observed in $Mn_{0.09}Ti_{1.1}S_2$ is due to clusters of intercalated Mn ions with an exponential size distribution. Monte Carlo investigations support the existence of an exponential cluster-size distribution and indicate that the clusters that give rise to this distribution are quasi-one-dimensional (chain-like). We note that very similar relaxation in the dielectric constant has been observed in the ferroelectric relaxors $Pb(Mg_{1/3}Nb_{2/3})O_3$ + 5% $PbTiO_3$ and $Pb_2KTa_5O_{15}$, which was explained on the basis of an exponential distribution of dipolar clusters.[19] In analogy with our findings for the $Mn_{0.09}Ti_{1.1}S_2$ magnetic systems, we posit that an exponential distribution of dipolar clusters in the ferroelectric relaxors is also due to chain-like or quasi-one-dimensional structures formed by the polar units.

II. EXPERIMENTAL DETAILS

Mn-intercalated $Ti_{1+y}S_2$ crystals were grown in a two-step process by the vapor-transport method using iodine as a carrier agent. The fabrication details have been discussed in previous

publications.[6, 20] After growth, the structural properties of the samples were investigated with powder x-ray diffraction (PXRD) and energy dispersive x-ray spectroscopy (EDX). The PXRD measurements were taken with Cu $K\alpha$ radiation on finely ground powder that had been passed through a 200-mesh (75-micron) sieve. The measurements showed that the samples were single-phase with a *c*-axis expansion consistent with a 9% Mn intercalation level.[21] The EDX measurements were taken on three or more larger single crystal samples with clean surfaces prepared by exfoliation in air just before the sample was mounted. Several readings were taken over the surface of each sample that was investigated. These measurements showed that the samples had formula unit $Mn_xTi_{1+y}S_2$, with $x = 0.09 \pm 0.02$ and $y \approx 0.1$. The Mn concentration was homogenous, but the measured Ti concentration could vary by as much as 5% over different crystals and even different areas of a single crystal. As mentioned before, excess Ti is invariably incorporated at intercalation during the growth of TiS_2 crystals. The extra Ti ions are located at intercalation sites with oxidation states of +4 or +3.

The $Mn_{0.09}Ti_{1.1}S_2$ sample used in our investigations consisted of a large number of very small single crystals (< 0.1 mm in every dimension) compacted in a cylindrical form. The mass of the sample was 0.1861 g. ac susceptibility and dc magnetization measurements were performed with a Quantum Design Physical Property Measurement System with the ac/dc magnetization option. The magnetic field was applied along the axis of the cylindrical sample. To check for orientational effects due to possible texture, test measurements were performed with the field perpendicular to the cylindrical axis. These measurements gave qualitatively identical behavior compared to the parallel orientation. Quantitative differences in magnetization were less than 5%. In performing all the measurements, we allowed enough time for thermal equilibration of the sample and sample chamber. When the sample was in "zero field," i.e., no

current in the superconducting magnet, the actual field experienced by the sample was the sum of the Earth's field and the remanent field of the magnet (<10 Oe). The field was oscillated to zero from a large value in order to achieve the lowest possible remanent field.

III. RESULTS AND DISCUSSION

Figure 1 shows the PXRD patterns for $Mn_{0.09}Ti_{1.1}S_2$ (black) and the host compound $Ti_{1+y}S_2$ (red), which was prepared using the same techniques as the Mn-intercalated material and hence contained self-intercalated Ti with $y \approx 0.1$. The (001), (002), and (003) peaks for $Mn_{0.09}Ti_{1.1}S_2$ are clearly shifted to the left (smaller angles) signifying a *c*-axis expansion induced by the intercalation of Mn. The relatively small change in the position of the (101) peak indicates that the in-plane lattice parameter *a* is almost completely unaffected by the intercalation of Mn. This is confirmed by analysis of the peak positions, which gives lattice parameter values of $a = 3.395 \pm 0.005$ Å and $c = 5.683 \pm 0.003$ Å for $Ti_{1+y}S_2$, and $a = 3.408 \pm 0.008$ Å and $c = 5.762 \pm 0.014$ Å for $Mn_{0.09}Ti_{1+y}S_2$. These values are consistent with those found in the literature.[21]

Figure 2 shows a graph of inverse susceptibility versus temperature for $Mn_{0.09}Ti_{1.1}S_2$. The Curie-Weiss law $\chi = C/(T - \Theta_{CW})$ is closely followed for temperatures $40\ \text{K} \le T \le 275\ \text{K}$, with $C = (3.47 \pm 0.01) \times 10^{-3}$ emu · K/(g · Oe) and $\Theta_{CW} = 8.3 \pm 0.2$ K. Using the experimental value $x = 0.09$, we find an effective Mn moment $p_{eff} = 6.1 \pm 0.6$, in agreement with the free-ion Mn^{2+} value of 5.92. (The fractional uncertainty in p_{eff} is somewhat large due to the propagation of the error in *x*.) The positive sign of Θ_{CW} indicates dominant ferromagnetic interactions. At

approximately 25 K, the $1/\chi$ data deviate slightly above the Curie-Weiss line, indicating the onset of short-range ferromagnetic order.[22]

The zero-field cooled magnetization (M_{ZFC}) and field-cooled magnetization (M_{FC}) for $Mn_{0.09}Ti_{1.1}S_2$ are plotted as functions of temperature in Fig. 3. The cooling (and measuring) field was 100 Oe. A bifurcation occurs at the irreversibility temperature $T_{irr} = 5.15 \pm 0.05$ K and the separation occurs very close to the peak in $M_{ZFC}(T)$. This coincidence of T_{irr} and T_{peak} is reminiscent of canonical spin glass (SG) behavior.[23-25] Note also that M_{FC} increases strongly at temperatures lower than the bifurcation point; this behavior is characteristic of cluster-glasses (CG) in systems with a high concentration of magnetic atoms.[23, 24] Thus, $M_{ZFC}(T)$ and $M_{FC}(T)$ of $Mn_{0.09}Ti_{1.1}S_2$ seem to interpolate between CG and canonical SG behavior.

To further investigate the nature of the magnetically glassy state, we measured T_{irr} as a function of applied field H. The graph of T_{irr} versus H is shown in Fig. 4. T_{irr} is a decreasing function of H as expected for spin glass-like materials. The mean-field theory of vector spin glasses with random anisotropy[26] predicts temperature-field transition lines described by the expression

$$T_g(H) = T_g(0)[1 - AH^p], \qquad (1)$$

where $T_g(0)$ is the transition temperature in zero applied field and A is a parameter that depends on the anisotropy, exchange, and the number of spin components. The anisotropy is assumed to be weak relative to the exchange. The value of the exponent p depends on the strength of the anisotropy relative to the magnetic field. In the strong-anisotropy regime, one finds $p = \frac{2}{3}$, which corresponds to the de Almeida-Thouless (AT) line for Ising spins. In the weak-anisotropy regime, $p = 2$, which defines the Gabay-Toulouse (GT) line. Using T_{irr} as a measure of the

transition temperature T_g,[27, 28] we fitted our data using Eq. (1). The best-fit values were $T_g(0) = 5.42 \pm 0.04$ K, $p = 0.57 \pm 0.02$, and $A = (3.7 \pm 0.7) \times 10^{-3}$ Oe$^{-0.57}$. The best fit line is shown in Fig. 4. At the highest magnetic field value used, the reduced field $h = \mu H / k_B T_g(0) < 0.16$; thus, h is small, as required. (We took $\mu = g\mu_B \sqrt{S(S+1)\mu_B^2/3}$.[29]) Clearly, the value of p for $Mn_{0.09}Ti_{1+y}S_2$ is quite close to $\frac{2}{3}$, suggesting an AT-like transition. The inset of Fig. 4 shows the fit when p is set at 0.67; the fit is still quite good. We infer that the intercalated Mn spin system exhibits relatively strong anisotropy (compared to h). Interestingly, the value of the exponent p obtained for $Mn_{0.25}Ti_{1+y}S_2$ was $\sim \frac{1}{3}$,[6] indicating less anisotropy than in $Mn_{0.09}Ti_{1+y}S_2$.

To gain more insight into the nature of the magnetic state below T_{irr}, we measured the ac susceptibility as a function of temperature in the vicinity of T_{irr} at different frequencies. The dc magnetic field was zero in all cases. Figure 5 shows the real part of the ac susceptibility (χ') versus temperature at several different frequencies ($30\ \text{Hz} \le f \le 10\ \text{kHz}$). The frequency dispersion for $T < T_{max}(f)$, where T_{max} is the temperature of the maximum in χ', is characteristic of relaxation in glassy (electric dipolar or magnetic) systems. Note that $T_{max} > T_{irr}$, a feature that is also characteristic of glassy systems. If we take T_{max} as the (frequency-dependent) spin-glass freezing temperature T_g, the shift in T_g with frequency as measured by the quantity $\Delta T_g / (T_g \Delta \log f)$ is found to be 0.017 ± 0.004. This value is at the upper end of the range for canonical spin glasses such as $Pd_{1-x}Mn_x$ and $Ni_{1-x}Mn_x$[30] and consistent with those of cluster glasses such as $CeNi_{1-x}Cu_x$.[23] The host materials for the $Pd_{1-x}Mn_x$ and $Ni_{1-x}Mn_x$ spin glasses are nearly ferromagnetic (Pd) or ferromagnetic (Ni) and therefore the Mn moments are likely to form

clusters even at very low concentrations.[31] Hence, the frequency shift of T_g is consistent with the presence of clustered Mn moments close to and below the spin freezing transition.

Figure 6 shows plots for the imaginary part of the ac susceptibility (χ'') versus temperature at various frequencies for $Mn_{0.09}Ti_{1+y}S_2$. The lowest-frequency data (30 Hz) are not shown because of the weakness of the out-of-phase signal at low frequencies. One observes that, like χ', the frequency and temperature dependencies of χ'' are similar to the behavior seen in glassy systems. $\chi''(f, T)$ is a sensitive probe of the nature of the low-temperature state because of its close relationship to the order parameter.[32, 33] In three-dimensional canonical spin glasses, $\chi''(f, T)$ obeys dynamic scaling based upon relaxation due to critical slowing down in the vicinity of the transition:[33, 34]

$$\chi'' T = \varepsilon^{\beta} F(f \varepsilon^{-z\nu}). \tag{2}$$

In Eq. (2), $\varepsilon = \left(T - T_C\right)/T_C$, T_C is the spin glass transition temperature, F is a scaling function, β is the critical exponent for the order parameter, and $z\nu$ is the product of the dynamic exponent and correlation-length critical exponent, respectively. In Fig. 7, we show our $\chi''(f, T)$ data plotted according to Eq. (2) with β, $z\nu$, and T_C as fitting parameters. Only data at temperatures above that of the peak in $\chi''(f, T)$ were included in the scaling plot.[33]. The best scaling was obtained for the following values: $T_c = 5.3 \pm 0.3$ K, $\beta = 0.8 \pm 0.6$ K, and $z\nu = 12 \pm 2$. The best collapse of the data was determined by fitting plots for a wide range of values of the parameters to a fourth-order polynomial and calculating the chi-squared statistic. The smallest value of χ^2 was obtained for the parameters given above. The uncertainties were obtained by considering parameter values for which the plots gave χ^2 values up to 1.5 times the minimum. There is good

overlap of the data only in a very narrow region around the abscissa value of 14. Further, the scaling was quite insensitive to the value of β. In addition, though $z\nu = 12$ produced the smallest value of χ^2, plots for larger values of $z\nu$ (i.e., less typical of SG systems) were frequently within the accepted χ^2 range. We conclude that scaling according to Eq. (2) is not satisfactory and hence the critical slowing down that characterizes continuous phase transitions in three dimensions provides an inadequate description of the glass-like transition in $Mn_{0.09}Ti_{1.1}S_2$. We further note that the qualitative behavior of $\chi''(f, T)$ for temperatures greater than the temperature at the peak is different from that of many spin glass and spin glass-like systems. For $Mn_{0.09}Ti_{1.1}S_2$, the decrease in χ'' as the temperature increases becomes steeper with increasing frequency, which is not the case in spin glass systems that exhibit power-law scaling due to critical slowing down.[34, 35] The qualitative behavior of $\chi''(f, T)$ for $Mn_{0.09}Ti_{1.1}S_2$ is more similar to that exhibited by the imaginary part of the dielectric permittivity in some ferroelectric relaxors,[19] which is likely an indication of deep underlying similarities in the nature of the interactions and the interacting entities in both systems.

The slow dynamics at a glass or glass-like transition may also be characterized by the Vogel-Fulcher (VF) relation[36, 37]

$$\tau = \tau_0 \exp\left[E / k(T - T_0)\right], \tag{3}$$

where τ is the relaxation time, τ_0 is a microscopic relaxation time, E is the activation energy and T_0 is the ideal glass temperature. In magnetic systems, the VF relation is thought to describe the relaxation of magnetic clusters that interact weakly.[36] For ferroelectric relaxors, the VF relation was derived semi-phenomenologically by assuming the polar nanoregions interact via

polarization of the surrounding medium to form clusters and that the mean cluster volume is a power-law function of the volume fraction of the polar nanoregions.[38] To ascertain the applicability of the VF law to $Mn_{0.09}Ti_{1.1}S_2$, we took $\tau = 1/f$ at $T = T_{max}$,[39, 40] where T_{max} is the temperature at which the maximum in $\chi'(f, T)$ occurs, and fit the τ versus T_{max} data using Eq. (3). The result is shown in Fig. 8. The best-fit values of the parameters are $\tau_0 = 1.2 \times 10^{-11}$ s, E = 1.2 meV (E/k = 14 K), and T_0 = 5.3 K. These values are physically reasonable and T_0 is very close to the value of $T_g(H = 0)$ = 5.42 K obtained from the dc magnetization data (see Fig. 4). Further, τ_0 is somewhat larger than typical single spin-flip times,[41] consistent with the existence of small magnetic clusters. Evidently, the VF law provides an excellent description of the data, which suggests that the magnetic units driving the glass-like transition in $Mn_{0.09}Ti_{1.1}S_2$ are clusters that interact relatively weakly. We remark that in many spin-glass systems, it is difficult to distinguish between VF behavior and critical slowing down, especially over relatively small frequency ranges.[42] However, even when both descriptions are seemingly equally effective in describing the relaxation behavior for the same system, the microscopic time τ_0 for the VF description in diluted systems (e.g., $\tau_0 > 10^{-8}$ s for $Cu_{0.954}Mn_{0.046}$) is often much larger than experimentally measured times.[42] Our value of τ_0 for $Mn_{0.09}Ti_{1.1}S_2$ is several orders of magnitude smaller than those obtained for diluted spin-glass systems such as $Cu_{0.954}Mn_{0.046}$. Further, as seen above, a power-law dynamic scaling description is inadequate for $Mn_{0.09}Ti_{1.1}S_2$. Thus, glass transitions in some systems (such as $Mn_{0.09}Ti_{1.1}S_2$) may not undergo a continuous phase transition and the VF law may provide the best description of the relaxation dynamics.

The frequency dispersion exhibited by $\chi'(f, T)$ and $\chi''(f, T)$ for $Mn_{0.09}Ti_{1.1}S_2$ indicates a distribution of relaxation times associated with the dynamical characteristics of the magnetic system. To describe the relaxation of polar clusters in ferroelectric relaxors, Lu and Calvarin[19]

assume an exponential distribution of sizes (volumes) and that the activation energy of each cluster is given by $E = KV$, where V is the volume of a cluster and K is the anisotropy constant. The relaxation of each cluster is governed by the Debye formula, with the relaxation time being thermally activated. Integrating over the distribution (with magnetic quantities substituted instead of electric ones) and assuming that $\omega\tau_c \ll 1$, where τ_c is the minimum relaxation time and $\omega = 2\pi f$, one finds that

$$\chi'' = -\left[\tan\left(\tfrac{n\pi}{2}\right)\right][\chi' - \Delta\chi], \tag{4}$$

where $n = kT/E_0$ and $\Delta\chi$ is the difference between the isothermal and adiabatic susceptibilities. Note that $E_0 = KV_0$, with V_0 being the width of the exponential size distribution. According to Eq. (4), if one plots a graph of χ'' versus χ' (Cole-Cole plot), one should obtain a straight line with slope $-\left[\tan\left(\tfrac{n\pi}{2}\right)\right]$, in contrast to archetypal Debye relaxation for which a semicircular Cole-Cole plot is obtained. In spin glasses, which possess a very wide distribution of relaxation times, the semicircle is flattened.[30] Figure 9 shows χ'' versus χ' graphs at two different temperatures, one for $T > T_g(H = 0)$ and the other for $T < T_g(H = 0)$. We note that excellent straight-line fits are obtained for the frequency range used, which though limited, is large enough to establish the existence of a significant linear regime. The good agreement between the experimental data and the model, in addition to the differences in behavior between $Mn_{0.09}Ti_{1.1}S_2$ and more-typical spin glass materials, strongly suggests that the cluster-glass transition in $Mn_{0.09}Ti_{1.1}S_2$ is unusual for disordered magnetic systems. An exponential distribution of magnetic clusters seems to be the driving force for this departure from more-standard spin glass characteristics.

We believe that the exponential distribution of magnetic clusters is a result of the self-intercalation of highly charged Ti ions (Ti^{3+}/Ti^{4+}) that reside in the van der Waals gaps along with the Mn^{2+} ions. To explore this idea further, we performed Monte Carlo simulations of the intercalated dichalcogenide system with variable concentrations of Ti and Mn intercalants. The Ti and Mn ions occupied sites on two-dimensional triangular lattices representative of intercalation sites. The lattice parameters used were derived from PXRD measurements to be a = 3.41 Å and the c-axis spacing increased with Mn concentration from c = 5.70 Å (x = 0) to c = 5.87 Å (x = 0.25). Each layer contained up to 900×900 sites; however, the main results were obtained from 200×200 and 72×72 systems. A simulated system consisted of up to five layers. To obtain various averages for the equilibrated systems as well as snapshots of likely configurations, we employed a classical Monte Carlo Metropolis algorithm based on a Hamiltonian consisting of a two-body screened-Coulomb potential

$$u_C = \frac{kq_i q_j}{r_{ij}} e^{-\Gamma r_{ij}}, \tag{5}$$

where r_{ij} is the separation between two intercalants having charges q_i and q_j., and Γ is the screening parameter. The value of Γ is taken to be 0.4 $Å^{-1}$ based upon transport measurements.[43]

Periodic boundary conditions were implemented in-plane and free boundary conditions were used along the c axis. Simulations were conducted for different lattice sizes to ensure that our results were independent of lattice size, and we found that the morphological features and behavior of 900×900 systems differed very little from those for the 200×200 systems, and the smallest reliable systems were about 72×72. The initial state of the system was a random occupation of lattice sites by Ti and Mn ions at their respective atomic concentrations. The temperature was then set to T = 1000 K (i.e., above the growth temperature) and the system

allowed to equilibrate after 100,000 Monte Carlo steps. The system was then annealed through T = 500 K to its low-temperature equilibrium state (T = 20 K).

Figure 10 shows the equilibrium atomic positions of Ti and Mn intercalants in the middle layer of a three-layer system with a Mn concentration of 9% and a Ti concentration of 10%, for computational cell sizes of 200×200 and 72×72 (inset). The Ti ions tend to form open structures to minimize their Coulomb energy and they are much more linear in multilayer systems, which suggests that out-of-plane interactions are influential in creating lower-dimensional symmetries. The Mn ions are forced to cluster in the spaces between these Ti chains; the effective dimensionality of the space occupied by the Mn is therefore reduced, which leads to the exponential cluster-size distribution as discussed below. We note that evidence for one-dimensional structures has been seen in $Mn_xTi_{1+y}S_2$ in atomic-force microscopy and scanning tunneling microscopy measurements.[44] Also, recall the increased anisotropy in $Mn_{0.09}Ti_{1+y}S_2$ compared to that in $Mn_{0.25}Ti_{1+y}S_2$ as indicated by the $M_{ZFC}(T)$ and $M_{FC}(T)$ measurements. This increased anisotropy is consistent with the shape anisotropy (and possibly enhanced magnetocrystalline anisotropy) associated with quasi-one-dimensional Mn clusters.[45] One-dimensional cluster growth has also been observed in simulations of colloidal systems in which particles interact via a short-range attractive force and a screened electrostatic repulsion.[46] In Fig. 11, we present graphs of number of clusters of a given size versus cluster size for a Mn concentration of 9% and a Ti concentration of 10% for system sizes of 72×72 and 200×200. Here, a cluster is defined to be a group of atoms in which each nearest-neighbor pair is separated by a distance slightly greater than $2a$, thereby encompassing the $2a \times 2a$ and $\sqrt{3}a \times \sqrt{3}a$ lattice spacings. The fit line for each system size is a simple exponential, which describes the cluster size distribution very well. Using a Gaussian function did not give as good a fit. We note that the

exponential distribution is obtained only for a relatively narrow range of concentrations of Mn and Ti: $7\% < x_{Mn} < 11\%$ and $5\% < y_{Ti} < 12\%$, with the widest Ti concentration range near 9% Mn coverage. In both Figs. 10 and 11, there is no fundamental difference in either the morphological features of the simulated systems or in their behavior, suggesting that finite size-effects are negligible. Systems smaller than 72×72 are not able to support the high aspect ratio clusters and therefore fail to capture this crucial feature of the system.

Assuming the magnetic clusters in $Mn_{0.09}Ti_{1.1}S_2$ are quasi-one-dimensional, a useful model for the cluster-size distribution is the random fragmentation of an infinite line in one dimension.[47] The fragments (clusters) follow the Poisson distribution if the occurrence of a fragment is random. The probability of finding a fragment of length between l and $l + dl$ is found to be

$$dP = N_0 e^{-N_0 l} dl, \tag{6}$$

where $1/N_0$ is average fragment length. Eq. (6) has precisely the exponential form assumed in the derivation of Eq. (4).[19] Clearly, however, the actual Mn clusters in $Mn_{0.09}Ti_{1.1}S_2$ will not be one-dimensional; they are presumably quasi-one-dimensional or chain-like. Thus, the simple exponential form is at best an approximation to the real cluster-size distribution and other distribution functions cannot be excluded. We plan to conduct magnetic small-angle neutron scattering experiments that will enable us to determine the spatial structure of the Mn clusters in $Mn_xTi_{1+y}S_2$ materials.

Finally, we comment on the occurrence of an exponential cluster distribution in ferroelectric relaxors such as $Pb(Mg_{1/3}Nb_{2/3})O_3$ (PMN). In PMN, x-ray diffraction and neutron scattering measurement on single crystals indicate the formation of nanoscale polar regions at low temperatures.[48] The polarization arises from displacements of the atoms relative to each

other within the perovskite structure. Not all atoms undergo such shifts; in fact, it was estimated that only 15–20% of the sample is occupied by this polar phase.[48] The polar nanoclusters are correlated over a distance of ~10 nm. It is also possible that the polar regions are chain-like or one-dimensionally correlated. Chain-like polar regions have been found in $PbZr_{1-x}Ti_xO_3$[49] and one-dimensionally correlated atomic shifts are present in the structurally frustrated relaxor ferroelectric $CaCu_3Ti_4O_{12}$.[50] Thus, though the shapes of the polar clusters in PMN have not been definitively established, we conjecture that the exponential distribution of polar clusters deduced from the frequency-dependent dielectric constant is also due to the quasi-one-dimensional structure of the clusters of polar nanoregions.

IV. CONCLUSIONS

We have investigated the nature of the low-temperature spin-glass-like phase in the intercalated dichalcogenide $Mn_{0.09}Ti_{1.1}S_2$ by means of dc magnetization and ac susceptibility. Weak deviation of the magnetic susceptibility from Curie-Weiss behavior as the temperature is lowered indicates the formation of small ferromagnetic clusters at low temperatures. The zero-field cooled magnetization and field-cooled magnetization when plotted as functions of temperature showed a bifurcation at a temperature T_{irr} near the peak of the ZFC plot. The FC magnetization continued to increase at temperatures below T_{irr}. A plot of T_{irr} versus applied magnetic field exhibited de Almeida-Thouless-like behavior, consistent with relatively strong anisotropy. ac susceptibility measurements in the vicinity of $T_{irr}(H = 0)$ exhibited frequency-dependent peaks in both χ' and χ'', suggesting spin-glass or cluster-glass behavior. Attempts to apply power-law scaling to the $\chi''(f, T)$ data resulted in relatively poor scaling, indicating that the transition was not

characterized by critical slowing down. On the other hand, an excellent fit to the data was obtained using the Vogel-Fulcher relation, with the physically reasonable parameter values $\tau_0 = 1.2 \times 10^{-11}$ s, E = 1.2 meV (E/k = 14 K), and T_0 = 5.3 K. The applicability of the Vogel-Fulcher relation represents additional evidence that the magnetic system at low temperatures consists of clusters, which interact to bring about the glass-like transition. The frequency dependence of the ac susceptibility in the cluster-glass regime of $Mn_{0.09}Ti_{1.1}S_2$ results from a distribution of relaxation times. This relaxation-time behavior is well described by an exponential distribution of cluster sizes, which was also found by Lu and Calvarin to provide an excellent description of dielectric relaxation in some ferroelectric relaxors. Noting that there is a significant degree of self-intercalation of Ti in the preparation of pure and intercalated TiS_2, we constructed a Monte Carlo model of the $Mn_xTi_{1+y}S_2$ system with varying concentrations of Mn^{2+} and Ti^{3+}or Ti^{4+} intercalants. It was found that an exponential distribution of cluster sizes occurred for a narrow range of concentrations of both species of intercalant ions. In this concentration regime, the highly charged Ti ions tended to form linear structures, which caused the magnetic Mn ions to cluster in chain-like forms. We conjecture that the quasi-one-dimensional Mn clusters lead to the exponential distribution of cluster sizes deduced from the experimental data. Such one-dimensional structures have been experimentally observed in dielectric systems with ferroelectric correlations, which may explain the similarity of the relaxation-time characteristics in ferroelectric relaxor systems and $Mn_{0.09}Ti_{1.1}S_2$.

ACKNOWLEDGMENTS

This work was supported by NSF Grant No. DMR 0504177, Iowa Office of Energy Independence Award No. 09-IPF-11, and Battelle.

REFERENCES

1 R. H. Friend and A. D. Yoffe, Adv. Phys. **36**, 1 (1987).
2 M. Inoue, H. P. Hughes, and A. D. Yoffe, Adv. Phys. **38**, 565 (1989).
3 Y. Tazuke, J. Magn. Magn. Mater. **140**, 155 (1995).
4 Y. Tazuke and T. Takeyama, J. Phys. Soc. Jpn. **66**, 827 (1997).
5 M. Sasaki, A. Ohnishi, T. Kikuchi, M. Kitaura, K.-S. Kim, and H.-J. Kim, Phys. Rev. B **82**, 224416 (2010).
6 P. M. Shand, T. Rash, M. Streicher, T. E. Kidd, K. R. Boyle, and L. H. Strauss, Phys. Rev. B **82**, 214413 (2010).
7 E. Morosan, H. W. Zandbergen, B. S. Dennis, J. W. G. Bos, Y. Onose, T. Klimczuk, A. P. Ramirez, N. P. Ong, and R. J. Cava, Nature Phys. **2**, 544 (2006).
8 E. Morosan, L. Li, N. P. Ong, and R. J. Cava, Phys. Rev. B **75**, 104505 (2007).
9 S. L. Bud'ko, P. C. Canfield, E. Morosan, R. J. Cava, and G. M. Schmiedeshoff, J. Phys.: Condens. Mat. **19**, 176230 (2007).
10 S. S. P. Parkin and R. H. Friend, Phil. Mag. B **41**, 65 (1980).
11 S. S. P. Parkin and R. H. Friend, Physica B **99**, 219 (1980).
12 M. Inoue, M. Matsumoto, H. Negishi, and H. Sakai, J. Magn. Magn. Mater. **53**, 131 (1985).
13 H. Negishi, H. Takahashi, and M. Inoue, J. Magn. Magn. Mater. **68**, 271 (1987).
14 K. Motizuki, N. Suzuki, and S. Tomishima, J. Magn. Magn. Mater. **104**, 681 (1992).
15 Y. Tazuke, T. Miyashita, H. Nakano, and R. Sasaki, Phys. Stat. Sol. C **3**, 2787 (2006).
16 R. M. A. Leith and J. C. J. M. Terhell, in *Preparation and Crystal Growth of Materials with Layered Structures*, edited by R. M. A. Leith (D. Reidel, Dordrecht, 1977), p. 162.
17 M. Inoue, M. Koyano, H. Negishi, Y. Ueda, and H. Sato, Phys. Stat. Sol. B **132**, 295 (1985).
18 M. Inoue, H. Negishi, T. Fujii, K. Takase, Y. Hara, and M. Sasaki, J. Phys. Chem. Solids **57**, 1109 (1996).
19 Z. G. Lu and G. Calvarin, Phys. Rev. B **51**, 2694 (1995).
20 T. E. Kidd, B. I. Gamb, P. I. Skirtachenko, and L. H. Strauss, Langmuir **26**, 10980 (2010).
21 M. Inoue and H. Negishi, J. Phys. Chem. **90**, 235 (1986).
22 A. Morgownik and J. Mydosh, Phys. Rev. B **24**, 5277 (1981).
23 N. Marcano, J. C. Gomez Sal, J. I. Espeso, L. Fernandez Barquin, and C. Paulsen, Phys. Rev. B **76**, 224419 (2007).
24 I. G. Deac, J. F. Mitchell, and P. Schiffer, Phys. Rev. B **63**, 172408/1 (2001).
25 L. Nagamine, B. Mevel, B. Dieny, B. Rodmacq, J. Regnard, C. Revenant-Brizard, and I. Manzini, J. Magn. Magn. Mater. **195**, 437 (1999).
26 G. Kotliar and H. Sompolinsky, Phys. Rev. Lett. **53**, 1751 (1984).
27 P. Beauvillain, C. Dupas, J. P. Renard, and P. Veillet, Phys. Rev. B **29**, 4086 (1984).
28 S. N. Kaul and S. Srinath, J. Phys.: Condens. Matter **10**, 11067 (1998).
29 N. de Courtenay, A. Fert, and I. A. Campbell, Phys. Rev. B **30**, 6791 (1984).
30 J. A. Mydosh, *Spin glasses: An experimental introduction* (Taylor and Francis, Washington, DC, 1993).
31 K. H. Fischer and J. A. Hertz, *Spin glasses* (Cambridge UP, Cambridge, 1991).

[32] P. M. Shand, A. D. Christianson, T. M. Pekarek, L. S. Martinson, J. W. Schweitzer, I. Miotkowski, and B. C. Crooker, Phys. Rev. B **58**, 12876 (1998).
[33] D. Bertrand, A. Mauger, J. Ferré, and P. Beauvillain, Phys. Rev. B **45**, 507 (1992).
[34] B. Leclercq, C. Rigaux, A. Mycielski, and M. Menant, Phys. Rev. B **47**, 6169 (1993).
[35] K. Gunnarsson, P. Svedlindh, P. Nordblad, L. Lundgren, H. Aruga, and A. Ito, Phys. Rev. Lett. **61**, 754 (1988).
[36] S. Shtrikman and E. P. Wohlfarth, Physics Letters A **85**, 467 (1981).
[37] A. K. Tagantsev, Phys. Rev. Lett. **72**, 1100 (1994).
[38] R. Pirc and R. Blinc, Phys. Rev. B **76**, 020101 (2007).
[39] J. Tholence, Solid State Communications **35**, 113 (1980).
[40] L. Lundgren, P. Svedlindh, and O. Beckman, J. Phys. F.: Met. Phys. **12**, 2663 (1982).
[41] P. Svedlindh, P. Granberg, P. Nordblad, L. Lundgren, and H. S. Chen, Phys. Rev. B **35**, 268 (1987).
[42] J. Souletie and J. L. Tholence, Phys. Rev. B **32**, 516 (1985).
[43] H. Negishi, H. Yamada, K. Yuri, M. Sasaki, and M. Inoue, Phys. Rev. B **56**, 11144 (1997).
[44] A. J. Stollenwerk, A. O'Shea, E. Wolter, M. W. Roth, L. H. Strauss, and T. E. Kidd, J. Phys. Chem. C **116**, 764 (2012).
[45] H. Neuendorf and W. Gunber, J. Magn. Magn. Mater. **151**, 305 (1995).
[46] F. Sciortino, P. Tartaglia, and E. Zaccarelli, J. Phys. Chem. B **109**, 21942 (2005).
[47] D. Grady and M. Kipp, J. Appl. Phys. **58**, 1210 (1985).
[48] N. de Mathan, E. Husson, G. Calvarin, J. Gavarri, A. Hewat, and A. Morell, J. Phys.: Condens. Mat. **3**, 8159 (1991).
[49] K. Rodeler and G. E. Kugel, Ferroelectrics **106**, 287 (1990).
[50] Y. Liu, R. L. Withers, and X. Y. Wei, Phys. Rev. B **72**, 134104 (2005).

Figure Captions

FIG. 1. (Color Online) Powder x-ray diffraction patterns for $Mn_{0.09}Ti_{1.1}S_2$ (black) and the host compound $Ti_{1+y}S_2$ (red). (001), (002), (003), (101), and (102) peaks are indicated for the purpose of comparison. The peaks for $Mn_{0.09}Ti_{1.1}S_2$ associated most with the *c* axis show the strongest shifts relative to undoped $Ti_{1+y}S_2$. Analysis of the peak positions shows that while the *c* axis spacing is significantly increased by Mn doping, the in-plane lattice constants are almost completely unaffected. The strong intensity of *c* axis peaks shows that the samples used for the XRD analysis have some texture; however, this has no effect on the determination of the lattice constants.

FIG. 2. (Color Online) Inverse susceptibility versus temperature for $Mn_{0.09}Ti_{1.1}S_2$. The Curie-Weiss law is obeyed for temperatures in the range $40\ \mathrm{K} \le T \le 275\ \mathrm{K}$ as illustrated by the solid line. At lower temperatures, there is a slight deviation from Curie-Weiss behavior, heralding the formation of small ferromagnetic clusters.

FIG. 3. (Color Online) Variation of the zero-field-cooled magnetization and field-cooled magnetization with temperature for $Mn_{0.09}Ti_{1.1}S_2$. The applied magnetic field is 100 Oe. The two data sets separate at the irreversibility temperature $T_{irr} = 5.15 \pm 0.05$ K.

FIG. 4. (Color Online) Bifurcation (irreversibility) temperature versus applied magnetic field for $Mn_{0.09}Ti_{1.1}S_2$. The solid line is a fit to Eq. (1) in text and the best-fit parameter values are shown. The exponent *p*, whose value gives an indication of the relative strength of the anisotropy, has

the best-fit value 0.57 ± 0.02. The inset shows the fit when the value of p is fixed at 0.67, which is the value expected in the "strong anisotropy" (AT-like) regime.

FIG. 5. (Color Online) Real part of the susceptibility (χ') versus temperature for $Mn_{0.09}Ti_{1.1}S_2$ for various frequencies. There is a frequency-dependent peak in χ' at temperatures somewhat higher than $T_g(H = 0)$, which is similar to the behavior exhibited by spin glasses and cluster glasses.

FIG. 6. (Color Online) Imaginary part of the susceptibility (χ'') versus temperature for $Mn_{0.09}Ti_{1.1}S_2$ for various frequencies. Note that the shape of the $\chi''(f,\ T)$ plots for temperatures greater than the temperature at the peak is somewhat different from the corresponding behavior for many spin glass and spin glass-like systems, particularly those that exhibit power-law scaling due to critical slowing down at near the transition.

FIG. 7. (Color Online) Power-law dynamics scaling plot for $Mn_{0.09}Ti_{1.1}S_2$ prepared using $\chi''(f,\ T)$ data plotted according to the scaling form given in Eq. (2). The frequencies used and the best-fit values of the critical temperature and scaling exponents are shown. The scatter in the plot indicates poor scaling, which in turn suggests that critical slowing down is not appropriate in describing the critical dynamical behavior.

FIG. 8. (Color Online) Relaxation time (taken to be $\tau = 1/f$) versus temperature T_{max} at the maximum of χ'. The solid line is a fit according to the Vogel-Fulcher law. The best-fit

parameters are $\tau_0 = 1.2 \times 10^{-11}$ s, E/k = 14 K, and T_0 = 5.3 K. Note that T_0 is very close to the value of $T_g(H = 0)$ = 5.42 K, attesting to the appropriateness of the Vogel-Fulcher description.

FIG. 9. (Color Online) χ'' versus χ' (Cole-Cole plot) for $Mn_{0.09}Ti_{1.1}S_2$. Each data point corresponds to a specific frequency $100\ \text{Hz} \le f \le 10\ \text{kHz}$. The upper graph represents data for T = 5.8 K [$>T_g(H = 0)$]; the lower one corresponds to T = 5.0 K [$<T_g(H = 0)$]. The linearity of the graphs is consistent with an exponential cluster-size distribution (see text).

FIG. 10. (Color Online) Results of equilibrated Monte Carlo simulations of intercalated TiS_2 for a 200×200 system showing positions of intercalated Ti ions (gold circles) and Mn ions (purple circles) in one layer for a Mn concentration of 9% and a Ti concentration of 10%. The layer shown is the middle layer in a three-layer system. The inset shows the results for a 72×72 system. The gold circles represent Ti ions and the blue circles denote Mn ions. Examples of linear structures formed by the Mn ions are surrounded by rectangles.

FIG. 11. (Color Online) Number of clusters of a given size versus cluster size for a Mn concentration of 9% and a Ti concentration of 10% according to a Monte Carlo simulation of intercalated TiS_2. Two layer sizes are shown: 72×72 and 200×200. A simple exponential function provides an excellent fit to the cluster-size distribution data for both system sizes.

Figure 1 - Shand

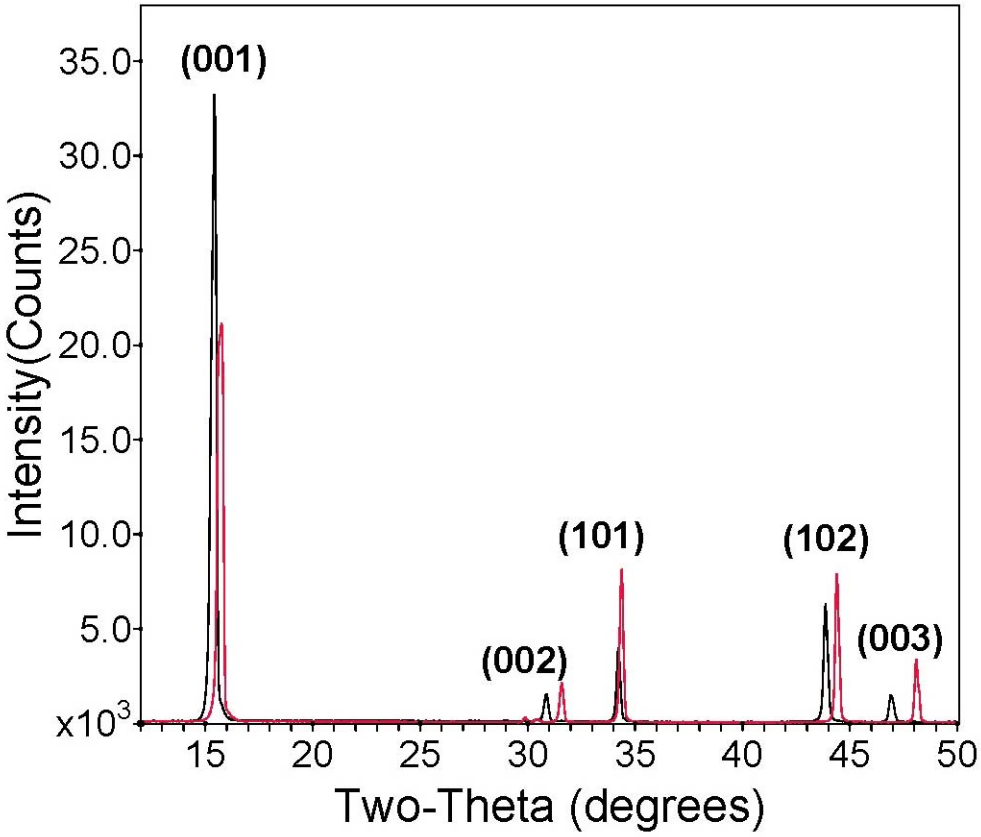

Fig. 1

Figure 3 - Shand

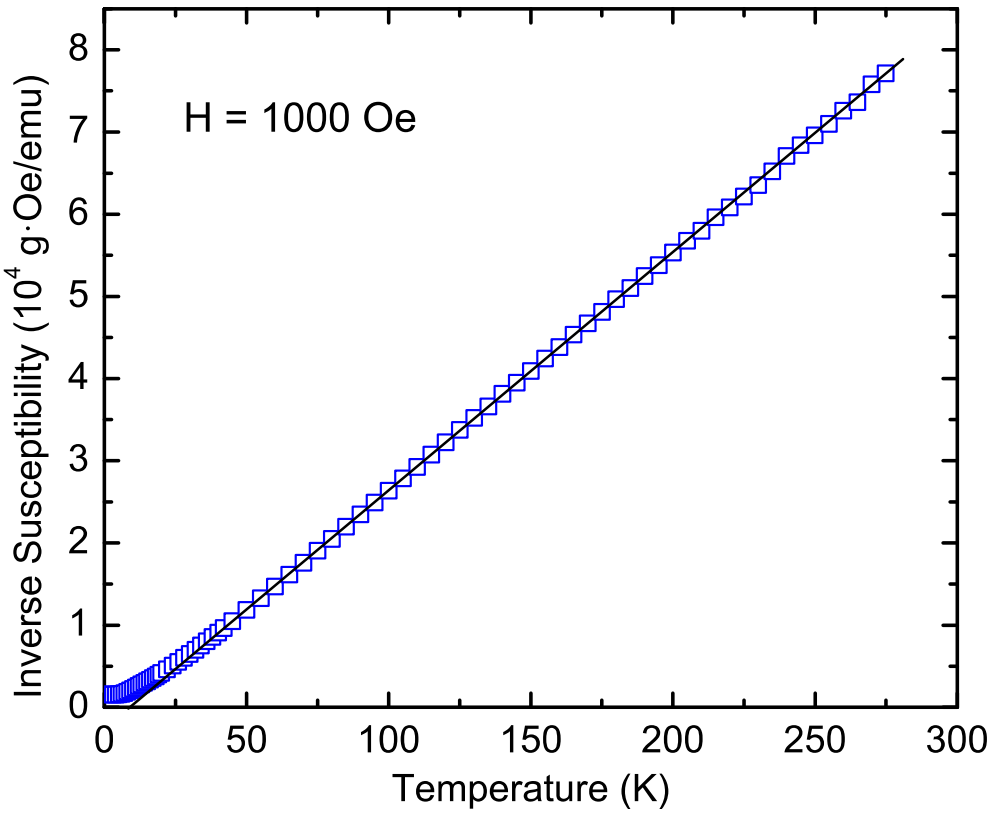

Fig. 2

Figure 2 - Shand

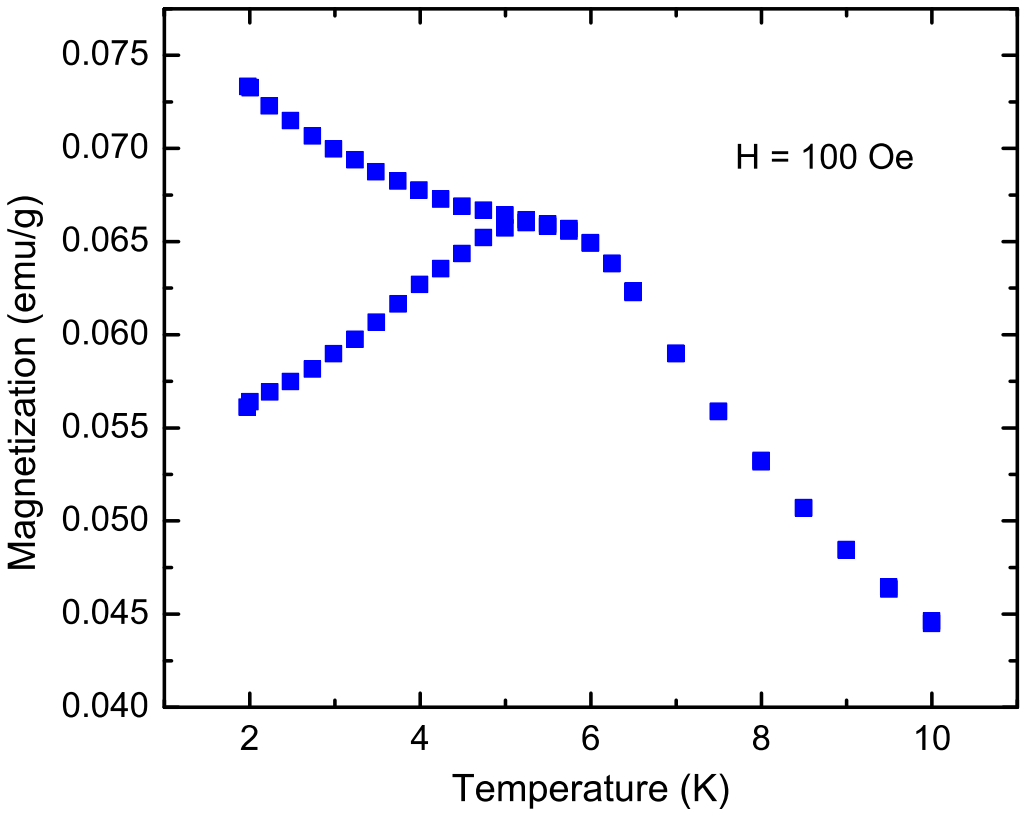

Fig. 3

Figure 4 - Shand

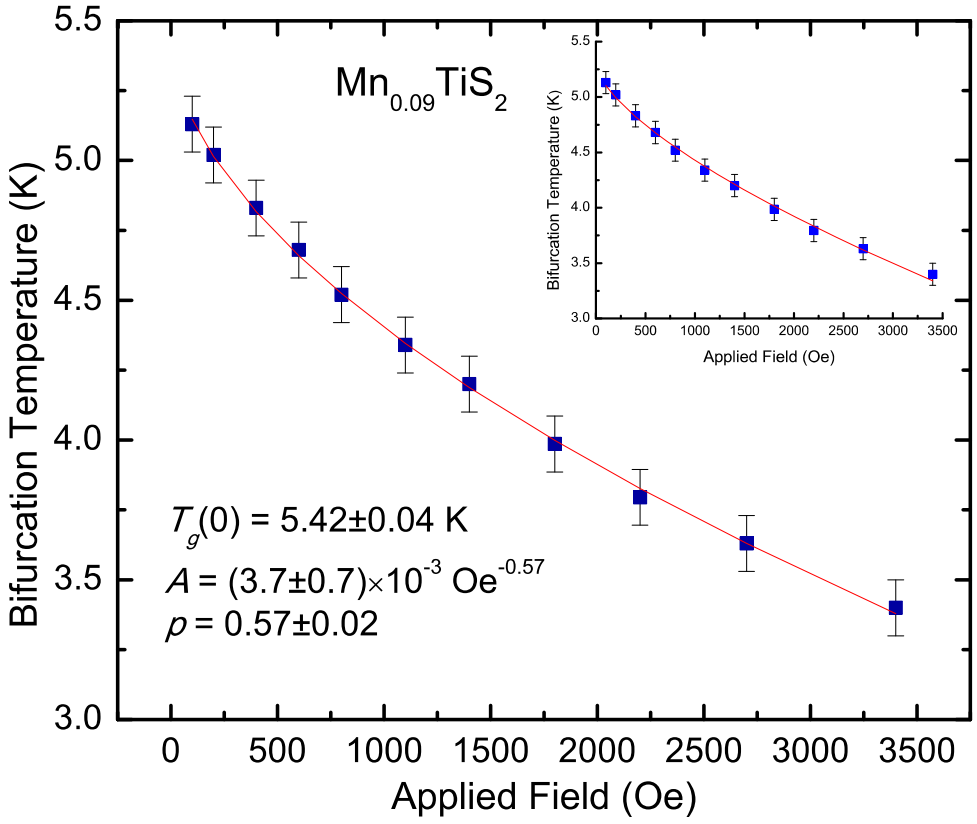

Fig. 4

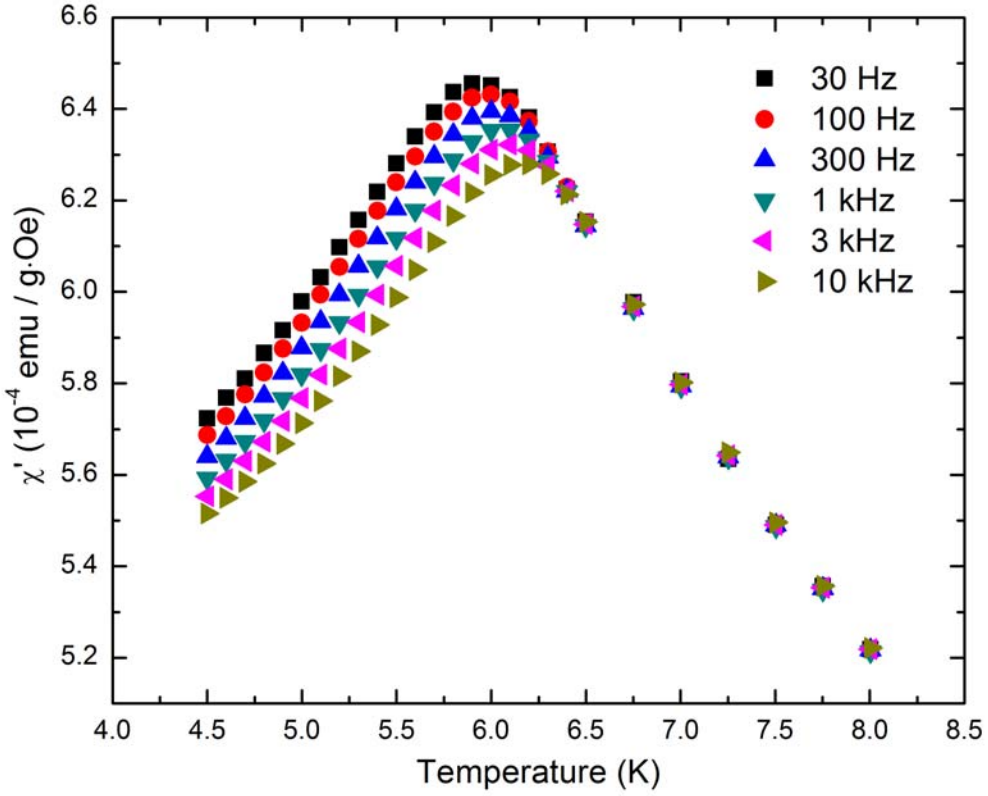
30 Hz
100 Hz
300 Hz
1 kHz
3 kHz
10 kHz
χ' (10^-4 emu / g·Oe)
Temperature (K)
6.6
6.4
6.2
6.0
5.8
5.6
5.4
5.2
4.0
4.5
5.0
5.5
6.0
6.5
7.0
7.5
8.0
8.5

Fig. 5

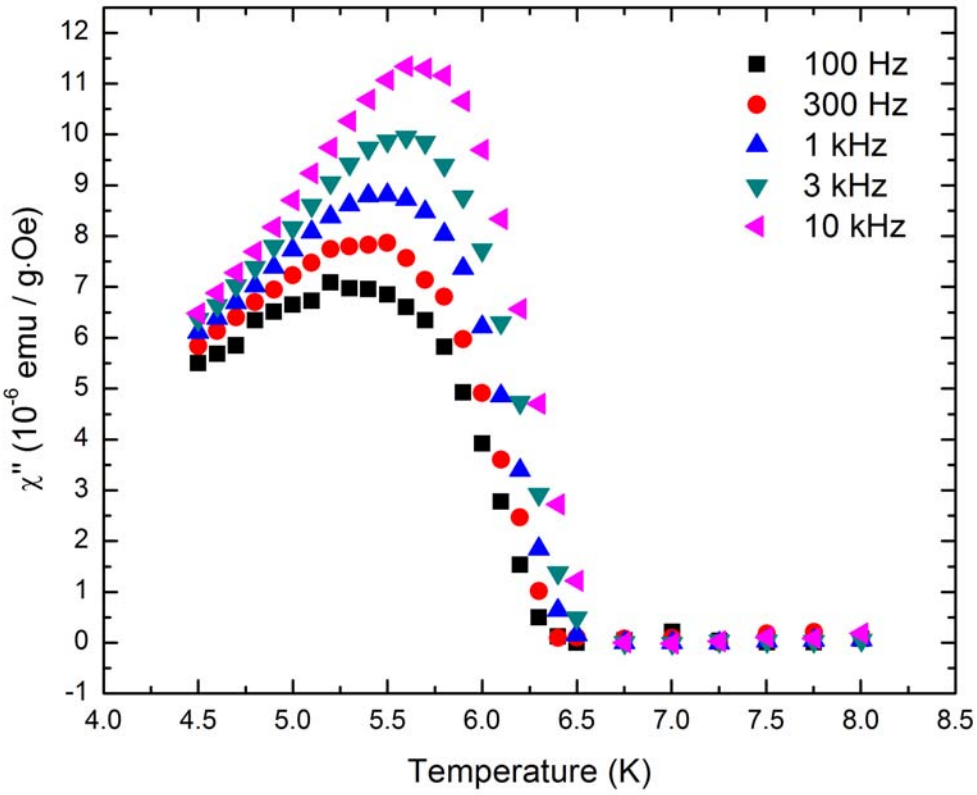
χ'' (10-6 emu / g·Oe)
Temperature (K)
100 Hz
300 Hz
1 kHz
3 kHz
10 kHz
12
11
10
9
8
7
6
5
4
3
2
1
0
-1
4.0
4.5
5.0
5.5
6.0
6.5
7.0
7.5
8.0
8.5

Fig. 6

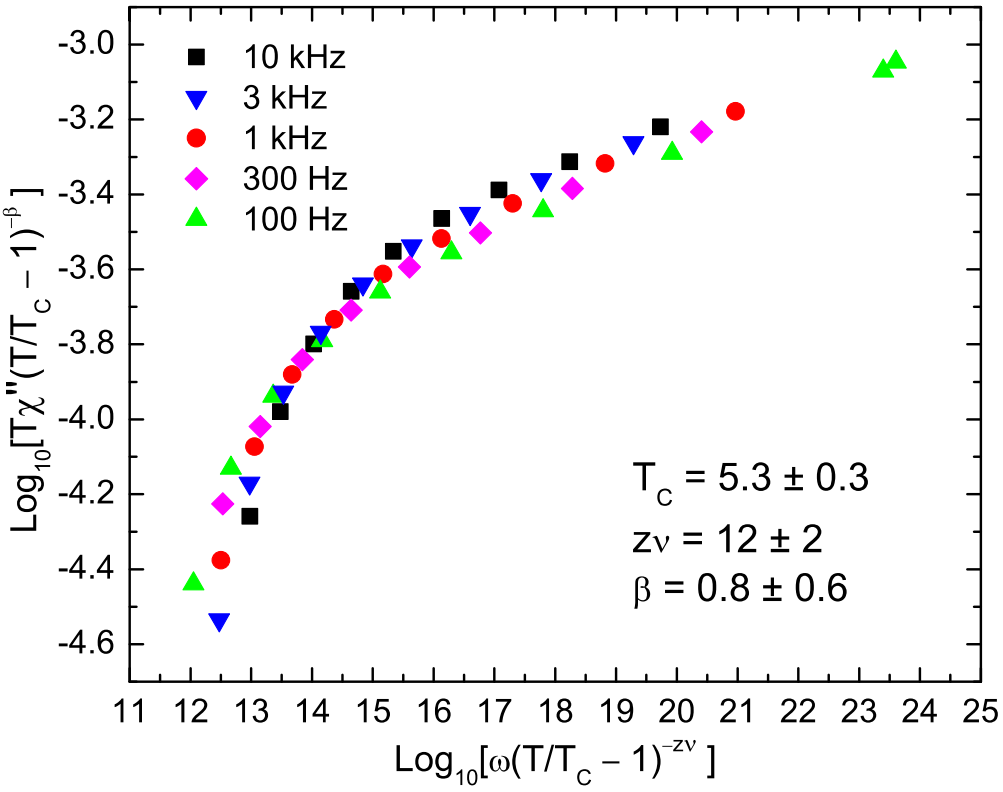
10 kHz
3 kHz
1 kHz
300 Hz
100 Hz
$T_C = 5.3 \pm 0.3$
$z\nu = 12 \pm 2$
$\beta = 0.8 \pm 0.6$
$Log_{10}[T\chi''(T/T_C - 1)^{-\beta}]$
$Log_{10}[\omega(T/T_C - 1)^{-z\nu}]$
-3.0
-3.2
-3.4
-3.6
-3.8
-4.0
-4.2
-4.4
-4.6
11 12 13 14 15 16 17 18 19 20 21 22 23 24 25

Fig. 7

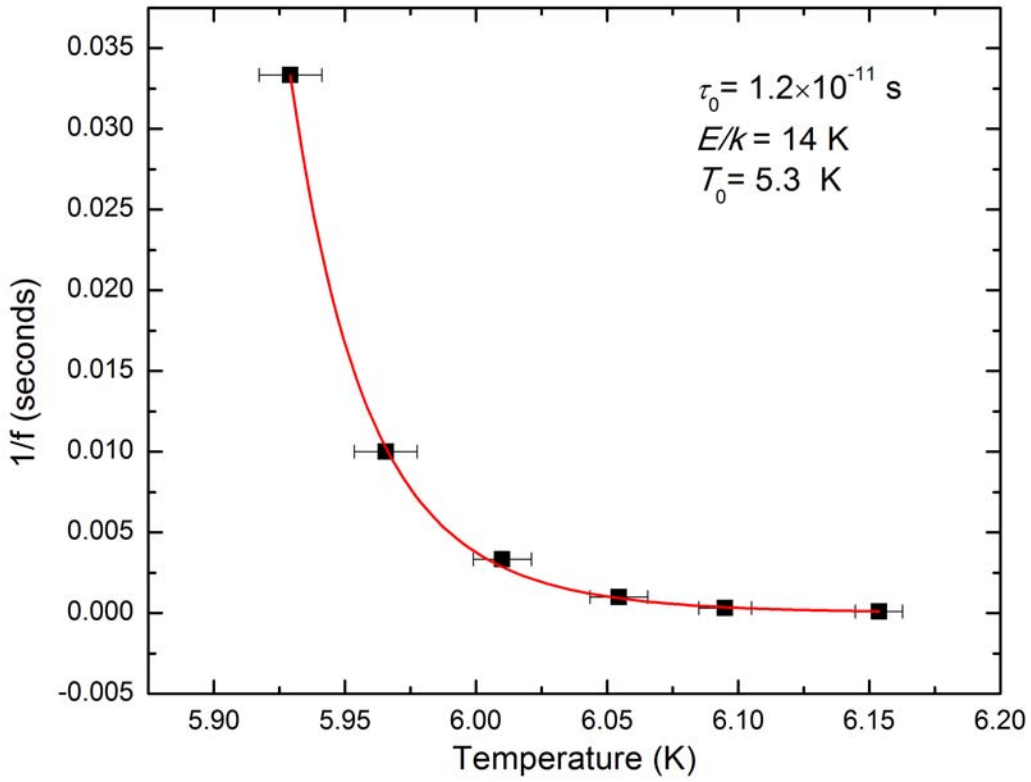
τ_0= 1.2×10^{-11} s
E/k = 14 K
T_0= 5.3 K
1/f (seconds)
Temperature (K)
0.035
0.030
0.025
0.020
0.015
0.010
0.005
0.000
-0.005
5.90
5.95
6.00
6.05
6.10
6.15
6.20

Fig. 8

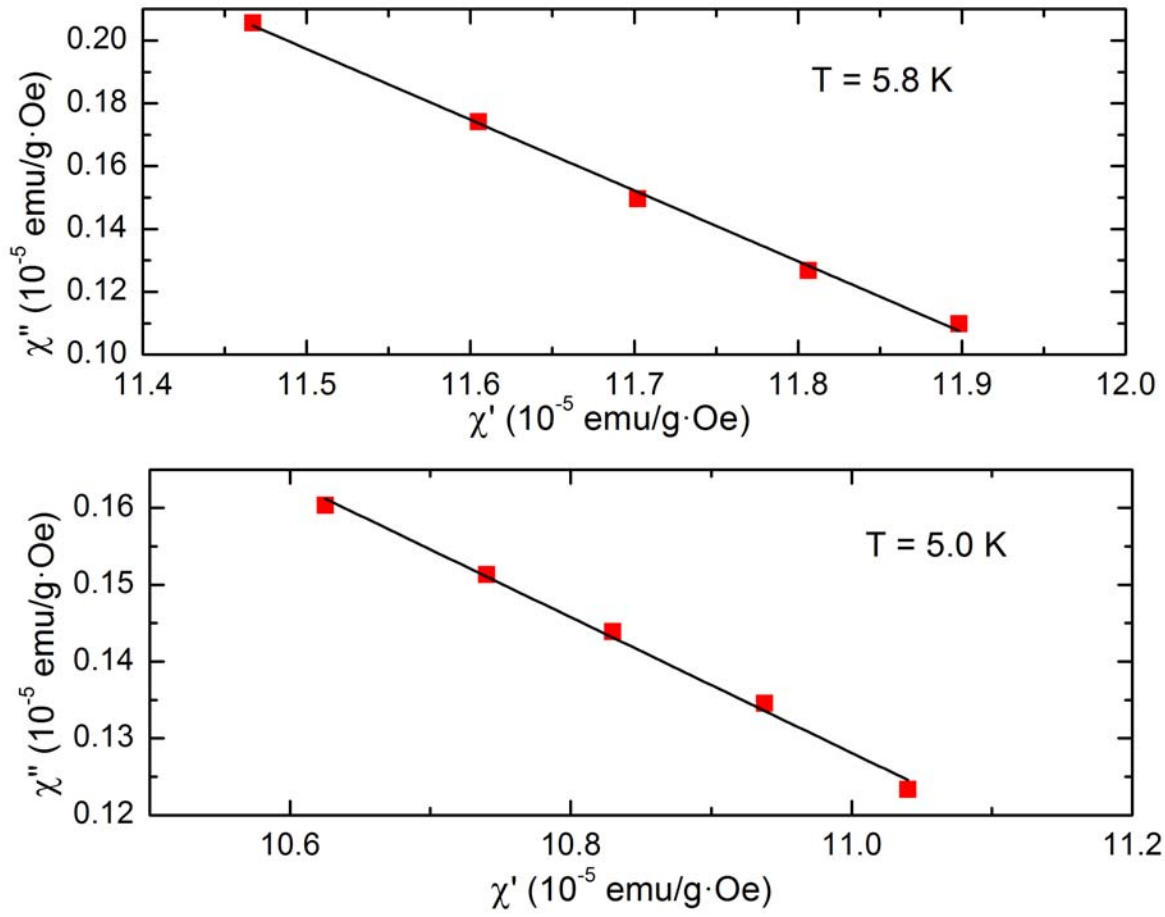
T = 5.8 K
χ'' (10^-5 emu/g·Oe)
χ' (10^-5 emu/g·Oe)
0.20
0.18
0.16
0.14
0.12
0.10
11.4
11.5
11.6
11.7
11.8
11.9
12.0
T = 5.0 K
χ'' (10^-5 emu/g·Oe)
χ' (10^-5 emu/g·Oe)
0.16
0.15
0.14
0.13
0.12
10.6
10.8
11.0
11.2

Fig. 9

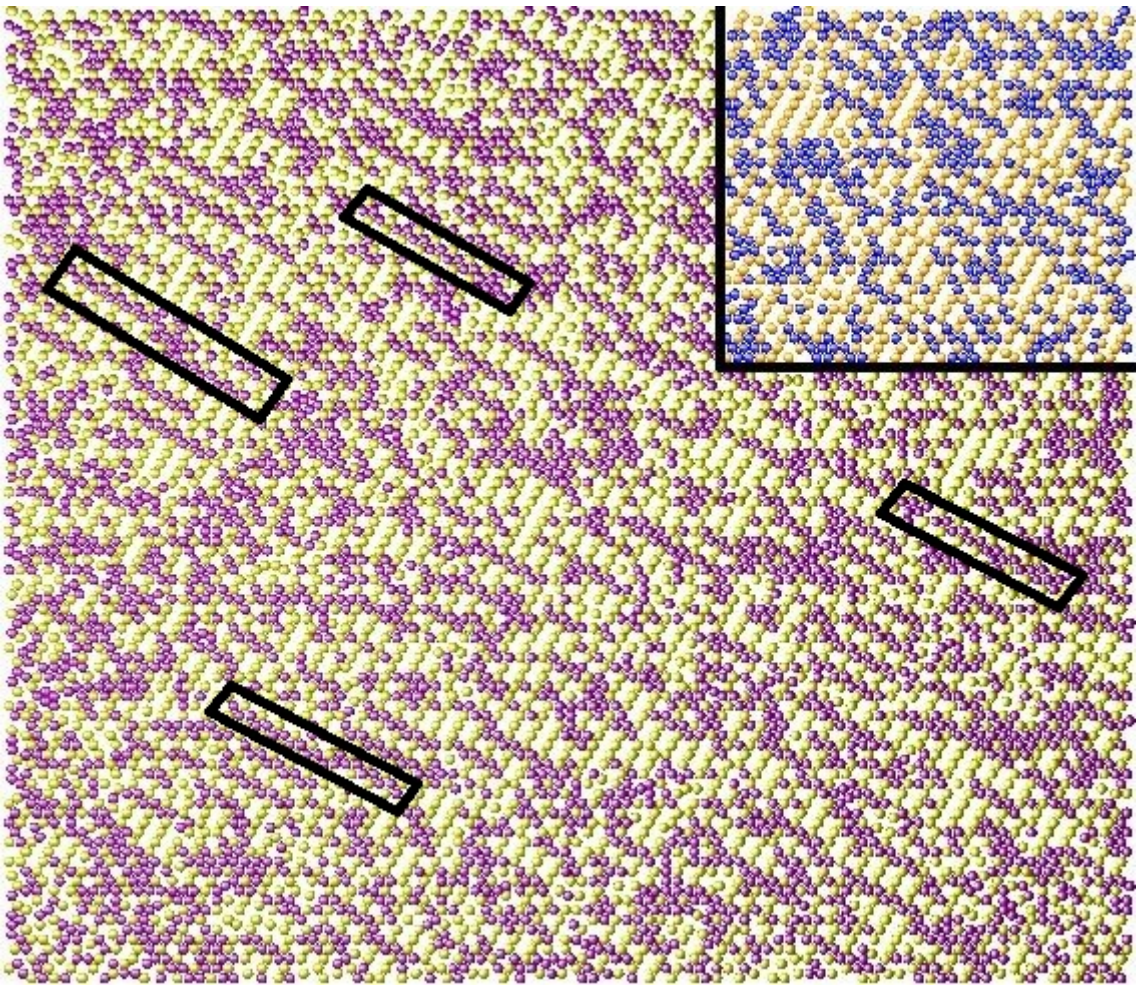

Fig. 10

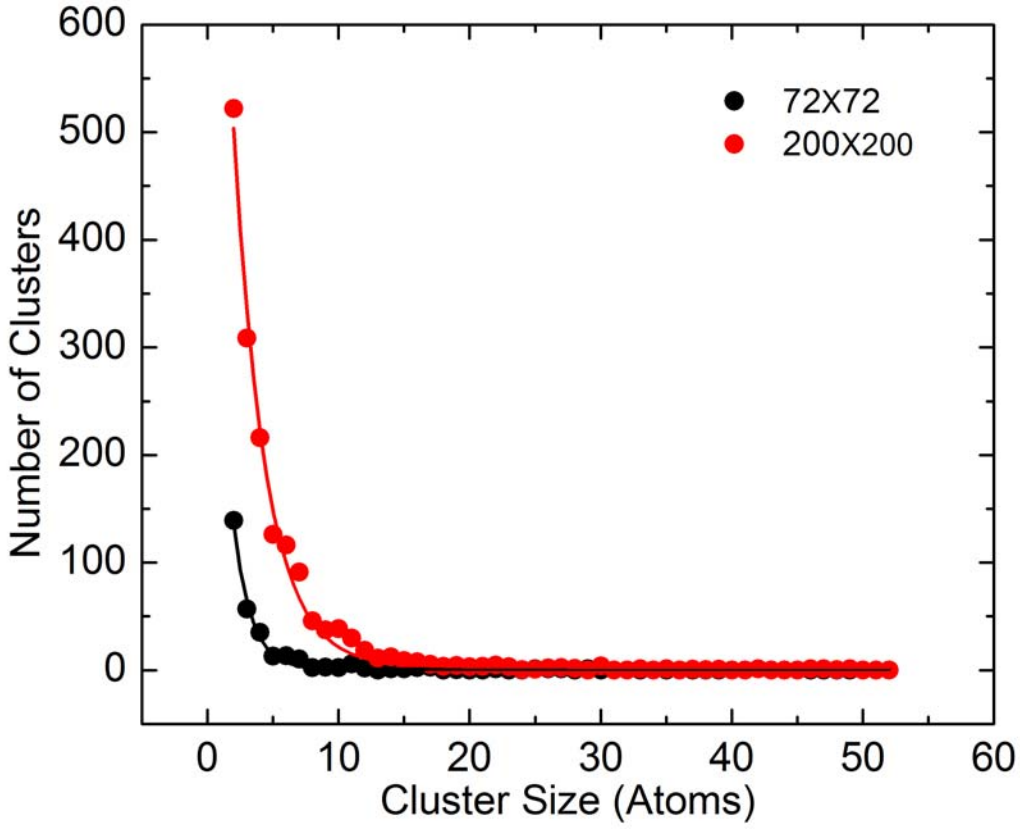
600
500
400
300
200
100
0
Number of Clusters
0
10
20
30
40
50
60
Cluster Size (Atoms)
72X72
200X200

Fig. 11